A monotonicity framework for stability verification of planar path-following controllers

Benton Clark and Hasan A. Poonawala

***Abstract*— This paper provides a new tool for verifying behavior of path-following controllers. Use of this tool involves evaluating the monotonicity of the controller with respect to the state. The resulting verification process is therefore simpler than Lyapunov-based methods. Moreover, the evaluation may be performed directly using observation data, without relying on a dynamics or sensor model to be learned. The verification is therefore practical in the context of data-driven control and feedback from information-rich sensors. Knowledge of dynamics or sensor models permits offline verification and design, as shown in several examples.**

***Index Terms*— Robotics; Nonholonomic systems; Stability of nonlinear systems; Autonomous vehicles; Data driven control.**

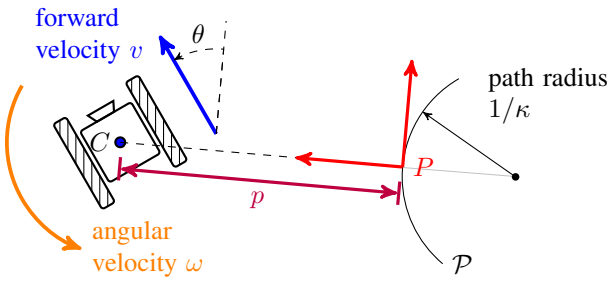

Fig. 1: A wheeled mobile robot (WMR) with forward speed v, and angular velocity ω. The curved black line represents a local segment of the path $\mathcal{P}$, with instantaneous path curvature κ, that the WMR must follow. The local Frenet-Serret frame (red) attached to the path is also shown. The WMR's state consists of the cross-track error p and angle θ with respect to the path.

I. Introduction

PATH-FOLLOWING for mobile robots using information-rich sensors like LiDAR or cameras is an important control application [1], [2]. A critical step in the control design is to certify that the path will be followed in some sense when using the sensor-controller combination. Lyapunov methods [3] are commonly used to show stability and convergence to the path due to the nonlinearity of the closed-loop system [4]–[10]. However, Lyapunov methods present two challenges. First, designers must often exploit details of the closed-form system equations to find valid Lyapunov functions, making the process highly specific to the dynamics and controller combination. Second, modeling closed-loop systems where information-rich sensors are part of the loop [2], [11] often relies on data-driven models of the sensor readings [12], [13]. Such sensor models are often too complicated for manual verification and highly specific to the environment in which the data are collected.

Recent research efforts try to leverage computational tools to overcome both the challenge of finding Lyapunov functions [14], [15] for nonlinear systems and the challenge of handling closed-loop models for sensor-based path-following controllers [12], [13]. These methods are often computationally expensive [12], and the guarantees are unlikely to be robust to changes in the model. The work in [14] reports a fast search for a Lyapunov function with some robustness to changes in path curvature, but it is unclear if their method will scale to closed-loop models that must account for sensing, as in [12]. Finally, these algorithms are typically incomplete, meaning they may fail to find a Lyapunov function even if one exists.

This paper develops a framework for path-following controller verification based on monotonicity of the closed loop dynamics terms with respect to the state. This framework can address the two limitations above. First, checking monotonicity does not rely on any candidate function, making it easier to apply than Lyapunov methods. Second, monotonicity of the closed-loop can sometimes be determined from monotonicity of the controller, as we show for some path-following systems. The latter can be verified online in an environment without access to a dynamics model or a sensor model, paving the way for practical verification of learned controllers using information-rich sensing. Availability of these models enables offline verification and design.

The main innovation is to define a target closed-loop dynamics model that enables proof of asymptotic stability even if exact closed-form expressions for some terms in the model are unavailable. Our choice of the target dynamics and the monotonicity conditions will enable straightforward verification of nonlinear path-following controllers in Section IV using different types of feedback and for different wheeled kinematics. Therefore, this paper provides a new and effective tool for path-following controller verification. Earlier work in [16] analyzed a specific control law and dynamics using stability in the sense of Lyapunov. Here, we use Poincare maps to analyze the target dynamics.

II. Path-Following Overview

A planar path $\mathcal{P}$ refers to a curve in the plane $\mathbb{R}^2$. We can express the kinematics of the robot in a local state-space representation known as the "orthogonal projection" [17,

*This work was supported by NSF-IIS-#2330794.

Benton Clark and Hasan A. Poonawala are in the Department of Mechanical and Aerospace Engineering, University of Kentucky, Lexington, KY 40506, United States {benton.clark,hasan.poonawala}@uky.edu

p.132] of the robot's centroid C about a path $\mathcal{P}$. The closest point P on $\mathcal{P}$ to centroid C defines a local Frenet-Serret frame, inducing path-local variables θ and p, with arc length s defining the 1D coordinate of P on $\mathcal{P}$. Variable p is the signed distance of the point P from the path, and θ is the difference between the heading direction of the mobile robot and the tangent to the path. The robot has a linear or forward velocity v and an angular velocity ω about C. Figure 1 depicts these quantities.

A generic curve will have a varying curvature $\kappa(s)$ along the path. Convergence to such a path is impossible without feed-forward control of the path. Therefore, we restrict our study to fixed-curvature paths, meaning $\kappa(s) \equiv \kappa$. Under fixed curvature, we obtain the following dynamics model for state $\vec{x} = (\theta, p)$:

$$\dot{p} = v \sin\theta, \text{ and} \tag{1}$$
$$\dot{\theta} = \omega - v\cos(\theta)\kappa/(1-\kappa p). \tag{2}$$

The **path-following problem** is to design a controller that specifies velocities v, ω that ensure that $p(t) \to 0$ as $t \to \infty$ and that $\dot{s}(t) > 0$ for all time.

The **path-following verification problem** is to verify that the designed controller will solve the path-following problem. This paper focuses on this second problem.

III. Target Closed-Loop Path-following System

Our goal is to present a simple and practical method for analyzing path-following controllers. We begin by formulating the path-following dynamics in Section II in terms of a *target* closed-loop dynamics for state $\vec{x} = (\theta, p)$:

$$\dot{p} = v(\theta, p)\, m(\theta), \text{ and} \tag{3}$$
$$\dot{\theta} = f_\theta(\theta, p), \tag{4}$$

where $m(\theta)$ is an odd function and $f_\theta(0,0) = 0$. These target dynamics assume that some feedback law $v(\theta, p)$ and $\omega(\theta, p)$ has been chosen and $\kappa(s) \equiv \kappa$. Furthermore, we **assume** that the functions $v(\theta, p)$, $m(\theta)$, and $f_\theta(\theta, p)$ are continuously differentiable. Under these assumptions, the origin is an equilibrium, and solutions to this system are well-defined and exist for all time.

Notation: We denote a specific state with a subscript, for example $\vec{x}_i = (\theta_i, p_i)$. The solution of (3)-(4) starting from initial condition $\vec{x}_0 \in D$ is $\vec{x}(t; \vec{x}_0) = (\theta(t; \vec{x}_0), p(t; \vec{x}_0))$, where t is time. When $\vec{x}_i$ is associated with a trajectory $\vec{x}(t; \vec{x}_0)$, then $\vec{x}_i = \vec{x}(T_i; \vec{x}_0)$. We denote the interior of set S by $\mathrm{Int}(S)$, the boundary of S by ∂S, and closure of S by $\overline{S}$. Finally, let Q_i denote the interior of the i^{th} quadrant:

$$Q_1 = \{\vec{x} \in \mathbb{R}^2 \colon \theta > 0,\ p > 0\},$$
$$Q_2 = \{\vec{x} \in \mathbb{R}^2 \colon \theta < 0,\ p > 0\},$$
$$Q_3 = \{\vec{x} \in \mathbb{R}^2 \colon \theta < 0,\ p < 0\}, \text{ and}$$
$$Q_4 = \{\vec{x} \in \mathbb{R}^2 \colon \theta > 0,\ p < 0\}.$$

Conditions under which the origin of (3)-(4) is asymptotically stable will become tools for stability verification as well as constraints on the control laws $v(\theta, p)$ and $\omega(\theta, p)$ designed for (1)-(2). The conditions are given by:

$$\frac{\partial f_\theta}{\partial \theta} < 0 \text{ and } \frac{\partial f_\theta}{\partial p} < 0 \forall \vec{x} \in \mathbb{R}^2, \tag{5}$$
$$\exists \alpha > 0 \text{ s.t. } v(\theta, p)\, m(\theta)\theta \geq \alpha\theta^2\ \forall \vec{x} \in \mathbb{R}^2, \text{ and} \tag{6}$$
$$\left|\frac{v(-\theta, p)}{f_\theta(-\theta, p)}\right| \geq \left|\frac{v(\theta, p)}{f_\theta(\theta, p)}\right|, \forall \vec{x} \in Q_1 \cup Q_3. \tag{7}$$

Condition (5) effectively implies that the angular velocity is monotonic in the states. Condition (6) requires that $\dot{p}$ depends in a reasonable way on the signs of v and θ, and cannot be small when θ is not. Condition (7) stipulates that the robot spins faster than it moves (smaller turning radius) when it is pointing away from the path ($\vec{x} \in Q_1 \cup Q_3$) compared to when it is pointing towards the path ($\vec{x} \in Q_2 \cup Q_4$).

Remark 1: When $v(\theta, p) \equiv v_c > 0$, a constant, and $m(\theta) = \sin\theta$, then (5) implies (6) and (7), but on a bounded subset of $\mathbb{R}^2$ where $|\theta| < \theta_{\max} < \pi/2$.

Condition (5) ensures that the set of points where $f_\theta(\theta, p)$ vanishes forms a curve that can be represented by a function $p = h(\theta)$:

Lemma 1: Let f_θ satisfy (5). Then, there exists a continuous function $h \colon \mathbb{R} \to \mathbb{R}$ such that the following conditions hold:

(i) $h(0) = 0$,
(ii) $f_\theta(\theta, h(\theta)) = 0$
(iii) h is strictly decreasing, and
(iv) Inverse h^{-1} exists.

Proof. Given condition (5), the implicit function theorem guarantees existence of a unique function $h(\theta)$ such that $f_\theta(\theta, h(\theta)) = 0$. Since $f_\theta(0,0) = 0$ in (4), therefore $h(0) = 0$. The derivative h' of h is

$$h'(\theta) = -\frac{\frac{\partial f_\theta}{\partial \theta}}{\frac{\partial f_\theta}{\partial p}},$$

which is strictly negative due to (5), and bounded under the assumption that f_θ is continuously differentiable. By integration, this strict negativity implies that h is strictly decreasing. Finally, since $h' < 0$, the inverse function theorem implies that $h^{-1} : \mathbb{R} \to \mathbb{R}$ exists. □

Lemma 1 allows us to divide $\mathbb{R}^2$ into two connected sets F_+ and F_- based on the sign of $f_\theta(\theta, p)$, with common boundary F_0:

$$F_+ = \{\vec{x} \in \mathbb{R}^2 \colon p < h(\theta)\},$$
$$F_0 = \{\vec{x} \in \mathbb{R}^2 \colon p = h(\theta)\}, \text{ and}$$
$$F_- = \{\vec{x} \in \mathbb{R}^2 \colon p > h(\theta)\},$$

where

$$(\theta, p) \in F_+ \iff f_\theta(\theta, p) > 0$$
$$(\theta, p) \in F_0 \iff f_\theta(\theta, p) = 0, \text{ and}$$
$$(\theta, p) \in F_- \iff f_\theta(\theta, p) < 0.$$

Conditions (5)-(6) will result in trajectories starting from the initial conditions of the form $(\theta_0, 0)$ to return to the θ-axis at an angle with sign opposite to that of θ_0, unless the

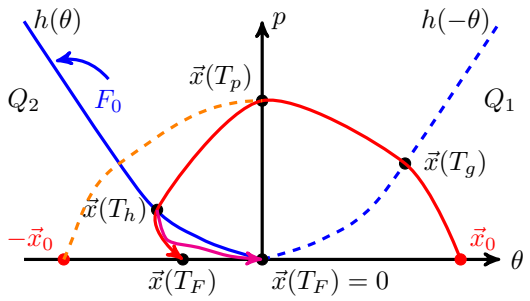

Fig. 2: A graphical illustration of Lemmas 3 and 4. The red trajectory represents a trajectory for which $T_F < \infty$. The magenta trajectory represents a trajectory in which $T_F = \infty$; the trajectory approaches the origin. The dashed orange line is the reflected curve in Lemma 4, which bounds the (red) trajectory in Q_2.

trajectory asymptotically reaches the origin. An example of such a trajectory is depicted in Figure 2. To prove the claim above, we need the following result.

Lemma 2: Consider the dynamical system $\dot{\vec{x}}(t) = f(\vec{x}(t))$ for $\vec{x}(t) \in \mathbb{R}$ where f is locally Lipschitz. If $f(\vec{x}) \leq -\epsilon < 0$ for all $\vec{x} \in [a, b]$ and some $\epsilon > 0$ then for any solution $\vec{x}(t; \vec{x}_0)$ where $\vec{x}_0 \in [a, b]$ $\exists T < \infty$ such that $\vec{x}(T) = a$.

Proof. The proof applies the Comparison Lemma [3]. Consider the dynamical system $\dot{u} = -\epsilon = \bar{f}(u)$ where $u(0) = b$ with state $u \in \mathbb{R}$. Then, $u(t) = b - \epsilon t$ and $u\left(\frac{b-a}{\epsilon}\right) = a$. For the system in $\vec{x}$, by assumption $\vec{x}_0 \leq u(0)$ and $\dot{\vec{x}} \leq \bar{f}(u(t))$ for any t. Therefore, by the Comparison Lemma, $\vec{x}(t) \leq u(t)$, which in turn implies that $\exists T$ such that $\vec{x}(t) = a$. □

We now prove that the claim above regarding the behavior of trajectories starting from θ-axis:

Lemma 3: If the system (3)-(4) satisfies conditions (5)-(6), then for every solution $\vec{x}(t; \vec{x}_0) = (\theta(t; \vec{x}_0), p(t; \vec{x}_0))$ where $\vec{x}_0 = (\theta_0, 0) \neq 0$ there exists $T_g < T_p < T_h < T_F \leq \infty$ such that

(i) $\vec{x}(t; \vec{x}_0) \in \overline{Q_1} \cup \overline{Q_3} \forall\ t \in [0, T_p]$,
(ii) $\theta(T_p; \vec{x}_0) = 0$ and $0 < |p(T_p; \vec{x}_0)| < \infty$,
(iii) $p(T_g; \vec{x}_0) = h(-\theta(T_g; \vec{x}_0))$,
(iv) $p(T_h; \vec{x}_0) = h(\theta(T_h; \vec{x}_0))$, and
(v) $p(T_F; \vec{x}_0) = 0$ and $0 \leq |\theta(T_F; \vec{x}_0)| \leq |\theta(T_h; \vec{x}_0)|$.

Proof. By symmetry about the θ-axis, the arguments for initial conditions where $\theta_0 > 0$ and will repeat for those where $\theta_0 < 0$, so we only consider the first case.

i) Trajectory enters Q_1:
By choice of $\vec{x}_0$, $\dot{p}(0) > 0$, therefore there exists sufficiently small $\epsilon > 0$ such that $\vec{x}(t; \vec{x}_0) \in Q_1$ for $t \in (0, \epsilon)$. Let $T_1 \in (0, \epsilon)$, so that $\vec{x}(T_1; \vec{x}_0) = \vec{x}_1 \in Q_1$.

ii) Trajectory reaches the positive p-axis:
We now show that the trajectory must reach the p-axis ($\{\vec{x} = (\theta, p) : \theta = 0\}$) in finite time, using a non-zero upper bound for $\dot{\theta}$. Let $Y = [a, b] \times [c, d] \subset \mathbb{R}^2$, where $a < b$ and $c < d$. The monotonicity condition (5) implies that for $(\theta, p) \in Y - \{(a, c), (b, d)\}$,

$$f_\theta(a, c) > f_\theta(\theta, p) > f_\theta(b, d). \tag{8}$$

We define $Y_1 = (0, p_1) \times (\theta_1, p_{\max})$. Due to (8), $0 > f(0, p_1) > f_\theta(\vec{x})$ for $\vec{x} \in Y_1$. If we define

$$\dot{\theta} = \bar{f}(\theta) = \max_{p_1 \leq p \leq p_{\max}} f_\theta(\theta, p),$$

by Lemma 2, we conclude that there exists finite $T > 0$ such that $\theta(T; \vec{x}_1) = 0$. For $t \in [T_1, T_p)$, $\vec{x}(t; \vec{x}_0) \in Q_1$, therefore $\dot{p}(t) > 0$ over this interval. As a consequence, $p(T_p; \vec{x}_0) > p_1 > 0$. Taking $T_p = T_1 + T$, we see that $\vec{x}_p$ lies on the positive p-axis. Since T_p is finite, $p(T_p; \vec{x}_0) < \infty$.

iii) Trajectory crosses $p = h(-\theta)$:
Since $p(T_p; \vec{x}_0) > h(-\theta(T_p; \vec{x}_0))$ and $p_0 < h(-\theta_0)$, by the intermediate value theorem, there exists T_g such that $p(T_g; \vec{x}_0) = h(-\theta(T_g; \vec{x}_0))$.

iv) Trajectory reaches line $p = h(\theta)$:
On a sufficiently small open set containing $\vec{x}_p$, $\dot{\theta} < 0$. Therefore, there exists $T > 0$ such that $\theta(T; \vec{x}_p) < 0$. Let

$$Y_2(\vec{x}_2) = \{(\theta, p) \in \overline{F_-} : \theta \leq \theta_2\},$$

for some $\vec{x}_2 \in Q_2$. The boundary of $Y_2(\vec{x}_2)$ is defined by F_0 and the line $\theta = \theta_2$. Given $\vec{x}_2 \in F_- \cap Q_2$, meaning that $\theta_2 < 0$ and $p_2 > h(\theta_2)$, for any $\vec{x} \in Y_2(\vec{x}_2)$,

$$\dot{p} \leq -\alpha|\theta_2| \text{ and } \dot{\theta} \leq 0.$$

Therefore, trajectories starting in $Y_2(\vec{x}_2)$ cannot exit through $\theta = \theta_2$. The derivative

$$\frac{d}{dt}(p - h(\theta)) = \dot{p} - h'(\theta)\dot{\theta} \leq -\alpha|\theta_2|$$

is strictly negative . By Lemma 2 , there must exist a finite time T' where $p(T'; \vec{x}_2) - h(\theta(T'; \vec{x}_2)) = 0$, which implies that $\vec{x}(T'; \vec{x}_2) \in F_0$. Taking $\vec{x}_2$ as $\vec{x}(T; \vec{x}_p)$, with T defined in the previous paragraph, we can define $T_h = T_p + T + T'$, so that $\vec{x}(T_h; \vec{x}_0) \in F_0$.

v) Trajectory reaches $p = 0$:
Consider the closed set $Y_3(\vec{x}_3) = \{\vec{x} \in \overline{F_+} \cap \overline{Q_2} : \theta \geq \theta_3\}$, for some $\vec{x}_3 \in \overline{F_+} \cap \overline{Q_2}$. The boundary of this set consists of three curves corresponding to subsets of F_0, $\theta = \theta_3$ and $p = 0$. For the trajectory $\vec{x}(t; \vec{x}_3)$ either there exists $T < \infty$ such that $t > T \implies \vec{x}(t; \vec{x}_3) \notin Y_3(\vec{x}_3)$, or $\vec{x}(t; \vec{x}_3) \in Y_3(\vec{x}_3)$ for all $t \geq 0$. If a finite T exists, then $\vec{x}(T; \vec{x}_3) \notin F_0 \cap Q_2$, since $\dot{p} < 0$ on this set but exiting through F_0 requires $\dot{p} > 0$. Similarly, $\theta(T; \vec{x}_3) \neq \theta_3$ since $\dot{\theta} \geq 0$ on the boundary of $Y_3(\vec{x}_3)$ corresponding to $\theta = \theta_3$. Therefore, if such a finite T exists, $\vec{x}(T; \vec{x}_3)$ must lie on the θ-axis. Moreover, $\theta(T; \vec{x}_3) \geq \theta_3$. If no such T exists, then $\vec{x}(t; \vec{x}_3) \in \text{Int}(Y_3(\vec{x}_3))$ for all $t > 0$. In that case, $\dot{p} < 0$ and $\dot{\theta} > 0$ for all $t > 0$. The only way for this situation to hold is that

$$\lim_{t \to \infty} \vec{x}(t; \vec{x}_3) = (0, 0).$$

Taking $\vec{x}_3 = \vec{x}_h$, and $T_F = T_h + T$ in the first case or $T_F = \infty$ in the second, we get $\theta(T_h; \vec{x}_0) \leq \theta(T_F; \vec{x}_0) \leq 0$. □

A useful consequence of Lemma 3 is as follows, which allows local asymptotic stability analysis.

Corollary 1: Any domain of the form

$$Y(\theta_{\max}, p_{\max}) = [-\theta_{\max}, \theta_{\max}] \times [-p_{\max}, p_{\max}], \tag{9}$$

where (5)-(7) are satisfied for all $\vec{x} \in Y(\theta_{\max}, p_{\max})$ contains a forward invariant subset containing the origin in its interior.

Proof. There must exist $\delta > 0$ sufficiently small such that both $\vec{x}(t;(\delta,0))$ and $\vec{x}(t;(-\delta,0))$ lie entirely within $Y(\theta_{\max}, p_{\max})$, otherwise Lemma 3 is contradicted. For any such δ, the solutions $\vec{x}(t;(\delta,0))$ and $\vec{x}(t;(-\delta,0))$ over their respective time intervals of the form $[0, T_p]$ and their reflections about the p-axis together define a forward invariant set that lies within $Y(\theta_{\max}, p_{\max})$. □

Lemma 3 is useful, but not sufficient. The quantity $|\theta(T_F;\vec{x}_0)|$ needs to be small enough, which the next result helps establish, through $|\theta(T_h;\vec{x}_0)|$.

Lemma 4: Let conditions (5)-(7) hold for system (3) and (4). Then

$$|\theta(T_h;\vec{x}_0)| \leq |\theta(T_g;\vec{x}_0)|. \tag{10}$$

Proof. The proof again looks at only one case, $\vec{x}_0 \in Q_1$, since the other case uses identical arguments. The idea in the proof is that the arc of the trajectory $\vec{x}(t;\vec{x}_0)$ from $[T_p, T_h]$ (red curve in Figure 2) must lie below the arc of the trajectory from $[T_g, T_p]$ when the latter is reflected about the p-axis (dashed orange curve in Figure 2). Due to the monotonicity of $h(\theta)$, this 'bound' on the former arc will imply (10). Lemma 3 ensures T_g, T_p, and T_h are well-defined.

By Lemma 3, for any initial condition $(\theta_0, 0)$ where $\theta_0 \neq 0$, $\theta(t;\vec{x}_0)$ is monotonic for $t \in [T_g, T_h]$. We can define an inverse function $T^{-1}(\theta;\vec{x}_0)$, so that

$$p(t;\vec{x}_0) = p(T^{-1}(\theta;\vec{x}_0);\vec{x}_0) := p(\theta;\vec{x}_0).$$

The reflected curve $\overleftarrow{p}(\theta;\vec{x}_0)$ is simply

$$\overleftarrow{p}(\theta;\vec{x}_0) = p(-\theta;\vec{x}_0).$$

We compare $\overleftarrow{p}(\theta;\vec{x}_0)$ and $p(\theta;\vec{x}_0)$ over the domain $[0, -\theta_h]$, by time-reversing the dynamics of p to get the dynamics for $\overleftarrow{p}$. We can derive the curves as solutions of the following ODEs over interval $[0, -\theta_h]$:

$$\frac{dp}{d\theta} = \frac{dp}{dt}\frac{dt}{d\theta} = \frac{v(\theta,p)\,m(\theta)}{f_\theta(\theta,p)} \leq 0, \text{ and} \tag{11}$$

$$\frac{d\overleftarrow{p}}{d\theta} = -\frac{v(-\theta,p)\,m(-\theta)}{f_\theta(-\theta,p)} = \frac{v(-\theta,p)\,m(\theta)}{f_\theta(-\theta,p)} \leq 0 \tag{12}$$

For $\vec{x} \in Q_1$, if (7) holds then

$$\frac{v(-\theta,p)\,m(\theta)}{f_\theta(-\theta,p)} \leq \frac{v(\theta,p)\,m(\theta)}{f_\theta(\theta,p)}.$$

By Lemma 2, $\overleftarrow{p}(\theta) \leq p(\theta)$ on $\theta \in [0, -\theta_h]$. Equivalently, $p(\theta) \leq \overleftarrow{p}(\theta)$ on $\theta \in [\theta_h, 0]$, as seen in Figure 2.

Now, $\exists 0 < \theta \leq \theta_g$ such that $\overleftarrow{p}(\theta) = h(-\theta_g)$, otherwise $\overleftarrow{p}(\theta_g) > p(\theta_g) = h(-\theta_g)$, contradicting the conclusion above. Since $\dot{p} < 0$ for $\vec{x} \in F_- \cap Q_2$, we must have $p_h \leq h(-\theta_g)$. Since h is strictly decreasing,

$$-\theta_g \leq \theta_h < 0.$$

By applying the same ideas to trajectories in $Q_3 \cup Q_4$, the proof is complete. □

The results above allow us to show global asymptotic stability of the origin.

Theorem 1: If the system described by (3) and (4) satisfies the conditions (5)-(7), then the origin is (globally) asymptotically stable.

Proof. Since conditions (5)-(7) hold, Lemmas 3 and 4 together imply that

$$|\theta_F| \leq |\theta_h| \leq \theta_g < \theta_0 \tag{13}$$

for any $\theta_0 \in \mathbb{R}$ where $\theta_0 \neq 0$. We can define the line $p = 0$ as a Poincare section. If θ^i is the i^{th} intersection, then (13) implies that $\theta^{i+1} < \theta^i$. As a result, iterates of the Poincare return map converge to the point $(0,0)$. Therefore, the origin is (globally) asymptotically stable. □

Therefore, conditions (5)-(7) guarantee global asymptotic stability of the origin of the target system (3) and (4). Theorem 1 can also be adapted to situations where the conditions are only shown to hold on a subset of $\mathbb{R}^2$:

Corollary 2: If conditions (5)-(7) hold on a subset of the form in (9), then the origin is locally asymptotically stable.

Checking condition (5) in a state does not require knowledge of that state, but (6) and (7) appear to. A simple way to overcome this dependence is to choose a constant forward velocity, as mentioned in Remark 1. Another way is to make $v(\theta,p)$ depend on (θ,p) through $\omega(\theta,p)$ (see Example 4).

IV. Examples

In this section, we apply the conditions from Section III to propose and analyze designs for path-following controllers under different scenarios. We aim to show that practical, but nonlinear, controllers are easily analyzed using the proposed framework. Examples 1-4 assume state-feedback, while Example 5 uses range-based sensing.

Figure 3 shows trajectories resulting from the controllers in each example. All parameters in the simulations have unit value, except $\kappa = 0.02\text{m}^{-1}$, $p_{\max} = 5\text{m}$, and $\gamma = \pi/3$ rad.

Example 1 (Differential drive, fixed curvature)**:** Differential drive robots have inputs that are exactly the velocities v and ω. We choose control laws for these inputs to be

$$v(\theta,p) = v_c, \text{ and} \tag{14}$$

$$\omega(\theta,p) = -\omega_c \tanh(k_\theta\theta + k_p p) + \omega_{FF}, \tag{15}$$

where v_c is a constant positive linear velocity, ω_c is a constant angular velocity, ω_{FF} is a constant feed-forward angular velocity, and k_θ, k_p are positive feedback gains. This control is a saturated linear feedback with a feed-forward term. The partial derivatives of the input $\omega(\theta,p)$ are

$$\frac{\partial\omega}{\partial\theta} = -\omega_c\left(1 - (\tanh(k_\theta\theta + k_p p))^2\right)k_\theta, \text{ and} \tag{16}$$

$$\frac{\partial\omega}{\partial p} = -\omega_c\left(1 - (\tanh(k_\theta\theta + k_p p))^2\right)k_p. \tag{17}$$

Clearly, the partial derivatives of ω with respect to both θ and p are negative for any $\vec{x} \in \mathbb{R}^2$.

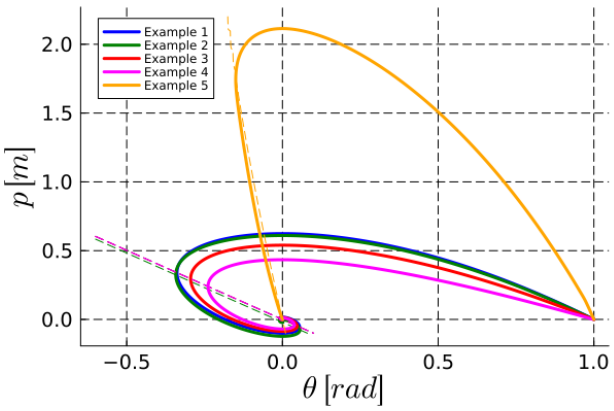

Fig. 3: Simulation results of the closed-loop systems in Examples 1-5 with initial condition $(1\text{rad}, 0\text{m})$. The state approaches the origin in all examples except for Example 2, as no feed-forward is used, where the equilibrium is $(0\text{rad}, -0.02\text{m})$. Dashed lines indicate the corresponding set F_0, which overlap for Examples 1, 3 and 4.

These control laws turn (1)-(2) into the closed-loop system

$$\dot{p} = v_c \sin\theta, \text{ and} \tag{18}$$

$$\dot{\theta} = -\omega_c \tanh\left(k_\theta \theta + k_p p\right) + \omega_{FF} - \frac{v_c \cos(\theta)\kappa}{(1-\kappa p)}, \tag{19}$$

where κ is the (fixed) curvature.

The partial derivatives of $f_\theta\left(\theta, p\right)$ (RHS of (19)) are

$$\frac{\partial f_\theta}{\partial p} = \frac{\partial \omega}{\partial p} - v_c \cos\theta \left(\frac{\kappa}{1-\kappa p}\right)^2, \text{ and} \tag{20}$$

$$\frac{\partial f_\theta}{\partial \theta} = \frac{\partial \omega}{\partial \theta} + v_c \sin\theta \frac{\kappa}{1-\kappa p}. \tag{21}$$

From (17) and (20), $\frac{\partial f_\theta}{\partial p} < 0$ for any $\vec{x} \in \mathbb{R}^2$. For $\frac{\partial f_\theta}{\partial \theta}$, the second term in (21) is sign indefinite. However, for any set $Y(\theta_{\max}, p_{\max})$ (see Equation (9)), where $p_{\max} < 1/\kappa$ and $\theta_{\max} < \pi/2$, if

$$\omega_c \left(1 - \left(\tanh\left(k_\theta |\theta_{\max}| + k_p |p_{\max}|\right)\right)^2\right) k_\theta > v_c \frac{|\kappa|}{1 - |\kappa| p_{\max}},$$

then $\frac{\partial f_\theta}{\partial \theta} < 0$ for $\vec{x} \in Y(\theta_{\max}, p_{\max})$.

When

$$\omega_{FF} = v_c \kappa,$$

then the origin is a unique equilibrium of (18) and (19), since the other terms in (19) are monotonic in p. Therefore, under inputs (14) and (15), the closed-loop dynamics (18) and (19) satisfies conditions (5)-(6). By Theorem 1, Remark 1, and Corollary 2, the origin is (locally) asymptotically stable.

Example 2 (No feed-forward angular velocity)**:** Consider Example 1 again. If $\omega_{FF} \neq v_c \kappa$, then the origin is not an equilibrium of (18) and (19). An equilibrium will be of the form $(0, p^*)$ where p^* must be a solution to the equation

$$-\omega_c \tanh\left(k_p p\right) + \omega_{FF} = v_c \frac{\kappa}{1-\kappa p}.$$

Since the left hand side (LHS) is monotonically decreasing in p and the RHS is monotonically increasing in p, for small enough v_c, such a p^* exists and is unique.

The dynamics can now be modified by transforming the state from (θ, p) to $(\theta, \bar{p})$ where $\bar{p} = p - p^*$, so that the resulting closed-loop system is.

$$\dot{\bar{p}}(\theta, \bar{p}) = v_c \sin\theta, \text{ and} \tag{22}$$

$$\dot{\theta}(\theta, \bar{p}) = \bar{f}_\theta = \omega(\theta, \bar{p}) - v_c \cos\theta \frac{\kappa}{1-\kappa \bar{p}}. \tag{23}$$

Following the same arguments in Example 1, if we choose ω and a domain $Y(\theta_{\max}, p_{\max})$ such that

$$\frac{\partial \omega}{\partial \theta} < -v_c \frac{\kappa}{1-\kappa p_{max}},$$

over that domain, where $p_{max} < 1/\kappa$ and $\theta_{\max} < \pi/2$, then the origin of the closed-loop dynamics (22) and (23) will be (locally) asymptotically stable. In turn, the original dynamics is ultimately bounded. Thus, the robot will converge to moving with a constant offset relative to the desired fixed curvature path.

Example 3 (Bicycle model)**:** For the bicycle model [8], [12], [14], $m(\theta) = \sin\theta$ again, but

$$f_\theta\left(\theta, p\right) = \frac{v\left(\theta, p\right)}{L} \tan\ \delta - \frac{v\left(\theta, p\right)\cos(\theta)\kappa}{(1-\kappa p)},$$

where L is the distance between the front and rear wheels, and δ is the steering angle of the front wheel, which is an input. If we use the same control law for v as in (14) but use the RHS of (15) as the law for control input δ, will the resulting system be asymptotically stable? Since the function tan is monotonically increasing on $(-\pi/2, \pi/2)$, we can see that the answer is automatically yes, but the origin's region of attraction is likely to be different, and equilibrium will be at $p^* \neq 0$ unless $\omega_{FF} = \tan^{-1}(L\kappa)$.

Example 4 (De-tuned linear velocity)**:** When v_c is large, the cross-track error p can increase significantly, which often implies a crash with objects near the path. However, reducing v_c makes the robot slow when aligned with the path. A practical solution is to use the following 'de-tuned' control law for $v\left(\theta, p\right)$, as done in [16]:

$$v\left(\theta, p\right) = v_c e^{(-\omega(\theta,p)^2)}. \tag{24}$$

Since $\omega\left(\theta, p\right)$ increases in magnitude with increase in θ for $\vec{x} \in Q_1 \cup Q_3$, and the exponential is strictly positive, conditions (6) and (7) will still hold on a similar region compared to that for when $v\left(\theta, p\right) \equiv v_c$. Figure 3 shows that $\max_t |p(t; \vec{x}_0)|$ reduces compared to Example 1.

Example 5 (Range-based feedback)**:** We analyze a robot that uses two range sensors, one pointed to the left and the other to the right, to navigate. The range sensors have an offset of magnitude γ with respect to the robot heading. If the distances returned by the left and right sensors are d_L and d_R respectively, the angular velocity control law is simply

$$\omega = 1/d_R - 1/d_L + \omega_{FF}, \tag{25}$$

where ω_{FF} is such that at $p = \theta = 0$, $\omega = v_c \kappa$. The control law (25) is easy to implement given range sensors, and avoids delays due to state estimation. Is it guaranteed to work?

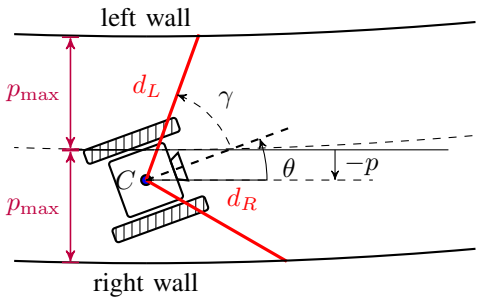

Fig. 4: A robot using two range sensors to navigate between two walls defining a curved corridor.

Figure 4 depicts this navigation strategy. Clearly, when the distance is measured from the left wall at a point ahead of the robot, increasing p and θ will decrease the measured distance. The opposite is true when measuring distance from the right wall. Therefore, when d_L and d_R are measured from the left and right walls respectively, ω in (25) is monotonically decreasing. Assuming $v(\theta, p) \equiv v_c$, we can again conclude (local) asymptotic stability to a fixed-curvature path using Theorem 1, Remark 1, and Corollary 2. While closed-form expressions are not required to come to this conclusion, we provide them below for completeness.

Zero curvature:

In a straight hallway of width $2p_{max}$, we can derive a closed-form expression for ω:

$$\omega = \begin{cases} \frac{\sin(\theta-\gamma)}{p_{\max}-p} - \frac{\sin(\gamma+\theta)}{p_{\max}-p} + v_c\kappa & \text{if } \theta > \gamma, \\ \frac{\sin(\gamma-\theta)}{p_{\max}+p} - \frac{\sin(\gamma+\theta)}{p_{\max}-p} + v_c\kappa & \text{if } |\theta| < \gamma, \text{ or} \\ \frac{\sin(-\theta+\gamma)}{p_{\max}+p} - \frac{\sin(-\gamma-\theta)}{p_{\max}+p} + v_c\kappa & \text{if } \theta < -\gamma. \end{cases}$$

One can check that $\frac{\partial f_\theta}{\partial \theta}$ and $\frac{\partial f_\theta}{\partial p}$ are strictly negative for $\theta \in (-\pi/2, \pi/2)$ and $|p| < p_{max}$. Therefore, the path defined by the center of the straight hallway is provably asymptotically stable under the sensor-driven controller (25).

Non-zero curvature:

Distances to the right and left wall are respectively given by

$$d_{rw}(x, y) = y\sin(x) + \sqrt{(R + p_{\max})^2 - y^2\cos^2(x)}, \text{ and}$$
$$d_{lw}(x, y) = y\sin(x) - \sqrt{(R - p_{\max})^2 - y^2\cos^2(x)},$$

where $R = 1/\kappa$, $y = R - p$, and $x = +\gamma$ for the left sensor and $x = -\gamma$ for the right sensor.

In all examples above, the robot converges to the desired circular path unless $\omega(0, 0) \neq v_c\kappa$, in which case the trajectories converge to an equilibrium $(0, p^*)$ which corresponds to a circular path with radius $|R - p^*|$.

V. Conclusion

This paper has proposed a method for analyzing planar path-following controllers that involves checking the monotonicity of control terms with respect to the state. As a consequence, it enables a simpler way to predict the effect of using a particular dynamics model (Example 3) or sensor (Example 5) for feedback, compared to Lyapunov-based approaches.

Some limitations of the work include 1) the inability to address time-varying closed-loop dynamics, which would capture environment properties like variable curvature, 2) the qualitative nature of Corollary 1, and 3) the reliance on closed-form sensor models or state-feedback in examples. Future work will address these limitations.

References

[1] N. Hung, F. Rego, J. Quintas, J. Cruz, M. Jacinto, D. Souto, A. Potes, L. Sebastiao, and A. Pascoal, "A review of path following control strategies for autonomous robotic vehicles: Theory, simulations, and experiments," *Journal of Field Robotics*, vol. 40, no. 3, pp. 747–779, 2023.

[2] A. Giusti, J. Guzzi, D. C. Cireşan, F.-L. He, J. P. Rodríguez, F. Fontana, M. Faessler, C. Forster, J. Schmidhuber, G. Di Caro, *et al.*, "A machine learning approach to visual perception of forest trails for mobile robots," *IEEE Robotics and Automation Letters*, vol. 1, no. 2, pp. 661–667, 2015.

[3] H. Khalil, *Nonlinear Systems*, ser. Pearson Education. Prentice Hall, 2002.

[4] S. Park, J. Deyst, and J. P. How, "Performance and lyapunov stability of a nonlinear path following guidance method," *Journal of Guidance, Control, and Dynamics*, vol. 30, no. 6, pp. 1718–1728, 2007.

[5] J. Kim, F. Zhang, and M. Egerstedt, "Curve tracking control for autonomous vehicles with rigidly mounted range sensors," in *2008 47th IEEE Conference on Decision and Control*, 2008, pp. 5036–5041.

[6] L. Lin and J. J. Zhu, "Line-of-sight pure pursuit guidance stability analysis and design guideline for car-like autonomous ground vehicles," ser. Dynamic Systems and Control Conference, vol. 3, 10 2019.

[7] Z. Li, O. Arslan, and N. Atanasov, "Fast and safe path-following control using a state-dependent directional metric," in *2020 IEEE International Conference on Robotics and Automation (ICRA)*, 2020, pp. 6176–6182.

[8] S. F. Campbell, "Steering control of an autonomous ground vehicle with application to the darpa urban challenge," Ph.D. dissertation, Massachusetts Institute of Technology, 2007.

[9] D. R. Nelson, D. B. Barber, T. W. McLain, and R. W. Beard, "Vector field path following for miniature air vehicles," *IEEE Transactions on Robotics*, vol. 23, no. 3, pp. 519–529, 2007.

[10] B. Rubí, R. Pérez, and B. Morcego, "A survey of path following control strategies for uavs focused on quadrotors," *Journal of Intelligent & Robotic Systems*, vol. 98, no. 2, pp. 241–265, 2020.

[11] K. Stachowicz, D. Shah, A. Bhorkar, I. Kostrikov, and S. Levine, "Fastrlap: A system for learning high-speed driving via deep rl and autonomous practicing," in *Conference on Robot Learning*. PMLR, 2023, pp. 3100–3111.

[12] J. A. Vincent and M. Schwager, "Reachable polyhedral marching (rpm): A safety verification algorithm for robotic systems with deep neural network components," in *2021 IEEE International Conference on Robotics and Automation (ICRA)*, 2021, pp. 9029–9035.

[13] H. A. Poonawala, N. Lauffer, and U. Topcu, "Training classifiers for feedback control with safety in mind," *Automatica*, vol. 128, p. 109509, 2021.

[14] A. Reed, G. O. Berger, S. Sankaranarayanan, and C. Heckman, "Verified path following using neural control lyapunov functions," in *Proceedings of The 6th Conference on Robot Learning*, ser. Proceedings of Machine Learning Research, K. Liu, D. Kulic, and J. Ichnowski, Eds., vol. 205. PMLR, 14–18 Dec 2023, pp. 1949–1958.

[15] P. Samanipour and H. A. Poonawala, "Stability analysis and controller synthesis using single-hidden-layer relu neural networks," *IEEE Transactions on Automatic Control*, vol. 69, no. 1, pp. 202–213, 2024.

[16] B. Clark, V. Hariprasad, and H. A. Poonawala, "Provably correct sensor-driven path-following for unicycles using monotonic score functions," in *2023 IEEE/RSJ International Conference on Intelligent Robots and Systems (IROS)*, 2023, pp. 354–360.

[17] C. C. d. Wit, H. Khennouf, C. Samson, and O. J. Sordalen, "Nonlinear control design for mobile robots," in *Recent trends in mobile robots*. World Scientific, 1993, pp. 121–156.